



# Preparation and Characterization of $\text{Bi}_2\text{MO}_6$ ( $\text{M} = \text{Mo}, \text{W}$ ) for Antibacterial Activity

<sup>1</sup>Huda N. Abid\*, <sup>2</sup>Amar Al-Keisy, <sup>1</sup>Duha S. Ahmed, <sup>3</sup>Sangeeta Singh

<sup>1</sup>Department of Applied Sciences, University of Technology – Iraq

<sup>2</sup>Nanotechnology and Advanced Materials Research Center, University of Technology – Iraq

<sup>3</sup>Microelectronics Lab, National Institute of Technology – India

## Article information

### Article history:

Received: July, 17, 2022

Accepted: September, 13, 2022

Available online: June, 10, 2023

### Keywords:

Bi-based photocatalysts,  
Hydrothermal approach,  
Nanosheets structure,  
Growth inhibition zone

### \*Corresponding Author:

Huda N. Abid

[as.18.88@grad.uotechnology.edu.iq](mailto:as.18.88@grad.uotechnology.edu.iq)

## Abstract

In recent years, Bi-based photocatalysts have begun to be applied in biological applications. However, the antibacterial ability of a Bi-based photocatalyst is still unclear. In this study,  $\text{Bi}_2\text{MoO}_6$  and  $\text{Bi}_2\text{WO}_6$  were successfully synthesized by a hydrothermal approach. The fabricated samples were characterized by X-Ray diffraction, FESEM, and UV-Vis spectra. Besides, the antibacterial activity of both photocatalyst samples toward *E. coli* as negative and *S. aureus* as positive pathogens were studied. Compared with antibacterial of  $\text{Bi}_2\text{WO}_6$ , the resultant  $\text{Bi}_2\text{MoO}_6$  exhibited high susceptible *S. aureus* bacterial strain revealing large zones of 24 mm to 29 mm, while  $\text{Bi}_2\text{WO}_6$  exhibited less susceptible of 17.5 mm to 21.5 mm as compared with the zone of inhibition against tested bacterial *E. coli*. Besides, a possible mechanism suggested the effect of nanosheet structure of samples to penetrate the cell membrane which results in leakage of interior cell and complete death and these results will provide some support for the applications of  $\text{Bi}_2\text{MoO}_6$  and  $\text{Bi}_2\text{WO}_6$  in antibacterial materials under common environments.

DOI: [10.53293/jasn.2022.5250.1179](https://doi.org/10.53293/jasn.2022.5250.1179), Department of Applied Sciences, University of Technology

This is an open access article under the CC BY 4.0 License.

## 1. Introduction

The deterioration of water quality caused by pathogenic has received public concern around the world. Besides, antibiotic accumulation in water has seriously become a great threat to environmental safety and human health [1]. As one of the most abundant bacteria in the environment, *E. coli* and *S. aureus* are always of great interest since they are pathogenic, harmless, and commonly found in food and water environment [1, 2]. Among the different fields, nanobiotechnology has represented an important research area with increasing the number of synthesis nanomaterials in several scientific studies as possible alternatives for resistance to pathogens [3]. In recent years, green, efficient, and cost-effective Bi-based semiconductor photocatalysts have emerged as a more promising methodology than conventional technology of bacterial inactivation methods such as UV disinfection and chlorination [4–7]. Because of its high stability, strong redox potential, low cost, and non-toxic nature,  $\text{TiO}_2$  has been extensively reported as an effective bactericidal semiconductor photocatalyst [8]. However, its band gap of 3.2 eV allows light absorption up to 387 nm, which accounts for just over 4% of the total solar spectrum.

Because visible light (47 %) in solar radiation is more abundant than UV, efficient visible-light photocatalysts are required to make the best use of this proportion [9]. Recently, the Bi-based semiconductor technology has been considered a promising alternative applicant to treat pathogenic microorganism pollution related to its various advantages like being clean, and, cost-efficient without generation of secondary pollution [3, 10]. Among these Bi-based photocatalysts, bismuth molybdates,  $\text{Bi}_2\text{MO}_6$  ( $M=\text{W}, \text{Mo}$ ) with the layered bismuth oxide family is of particular interest as a typical Aurivillius oxide due to its dielectric, ion-conductive, luminous, and catalytic properties [11–13]. A typical n-type semiconductor comprised of accumulating layers of alternating  $(\text{Bi}_2\text{O}_2)^{2+}$  layers and  $(\text{MO}_4)^{2-}$  octahedral sheets is also a promising visible-light-driven photocatalyst with good chemical and thermal stability, aside from its non-toxic and ecologically friendly nature [14, 15]. Moreover,  $\text{Bi}_2\text{MoO}_6$  can degrade organic contaminants and exhibit high antibacterial effects under visible light irradiation [16-17]. Besides, Bismuth tungsten  $\text{Bi}_2\text{WO}_6$ , representing the Bi-based photocatalysts, can produce strong oxidizing free radicals that inactivate microorganisms and is very suitable for antibacterial treatment.  $\text{Bi}_2\text{WO}_6$  has received much attention as active in visible light regions and is more useful for environmental treatment purposes [18]. Despite the catalyst's lengthy history as a potential solution, most research on  $\text{Bi}_2\text{MoO}_6$  has concentrated on the photocatalytic breakdown of organic pollutants, with only a few studies looking into the photocatalytic inactivation of microorganisms. A pseudo-first-order process observed *E.coli* degradation on  $\text{Bi}_2\text{MoO}_6$  nest-like structures in a few hours [19]. Both  $\text{Bi}_2\text{MoO}_6$  and  $\text{Bi}_2\text{WO}_6$  have outstanding visible light photocatalytic activity due to their superior geometrical structural features [14, 20]. Constructing a unique micro/nano hierarchical structure typically shortens the paths of water contaminants, absorbs incidental light more efficiently due to increased multiple scattering, and is easily separated from wastewater by filtering or sedimentation processes [15, 21]. In this paper, Bi-based semiconductors like  $\text{Bi}_2\text{MO}_6$  ( $M=\text{W}, \text{Mo}$ ) were synthesized by using the hydrothermal method. The antibacterial effects and the proposed mechanism of the resulting nanosheets against the standard and multidrug-resistant *E.coli* as gram-negative and *S.aureus* as gram-positive bacteria were investigated.

## 2. Experimental Part

### 2.1. Synthesis of $\text{Bi}_2\text{MoO}_6$ and $\text{Bi}_2\text{WO}_6$ Nanoparticles

Based on prior research [22], a two-step hydrothermal technique was used to manufacture nanoplate  $\text{Bi}_2\text{MoO}_6$  and  $\text{Bi}_2\text{WO}_6$ .  $\text{Bi}(\text{NO}_3)_3$  (2 mmol) was first dissolved in 10 mL of nitric acid solution ( $\text{HNO}_3$ ), then a 10-mL aliquot of  $\text{Na}_2\text{MoO}_4$  solution (1 mmol) was dissolved and dropped into the  $\text{Bi}(\text{NO}_3)_3$  solution while stirring. The blended solution's pH level was set at 4. The finished suspension was quickly transferred to a Teflon-lined 50-mL autoclave and cooked at  $180^\circ\text{C}$  for 15 hours in the second stage. Following that, the suspension was allowed to cool naturally at ambient temperature, and the solid result was cleaned multiple times before being dried in the air at  $60^\circ\text{C}$  for 24h.  $\text{Bi}_2\text{WO}_6$  nanoparticles were made using identical processes and amounts as  $\text{Bi}_2\text{MoO}_6$  nanoparticles, but instead of  $\text{Na}_2\text{MoO}_4$ ,  $\text{Na}_2\text{WO}_4$  was used.

### 2.2. Characterization

The XRD analysis of prepared samples was performed by Shimadzu X-ray diffraction 6000 diffractometer with  $\text{CuK}\alpha$  radiation ( $\lambda=1.542 \text{ \AA}$ ). Data were recorded in the  $2\theta$  range of  $10^\circ$ - $70^\circ$ . The band gap of the samples was recorded on a Shimadzu UV-1800 spectrophotometer and determined the optical properties. The surface morphology of samples was characterized by field emission scanning electron microscopy (FESEM, Mira3-XMU). The chemical composition of produced samples was determined by energy dispersive x-ray spectroscopy (EDS connected to FESEM).

### 2.3. Antibacterial Activity

The antibacterial activity of the resulting semiconductor like  $\text{Bi}_2\text{MO}_6$  ( $M=\text{W}, \text{Mo}$ ) was evaluated against *E.coli* as negative and *S.aureus* as positive pathogens by agar well diffusion assay [23, 24]. 25  $\mu\text{l}$  of *E.coli* and *S.aureus* cultures suspension were prepared with initial concentration  $10^6$  (CFU/ml, McFarland tube No.0.5) and incubated for 18h and spread on the Mueller Hinton agar surface poured in Petri plates. Holes of 6 mm were made, and each hole was packed with different test concentrations of samples ranging from 50, 100 and 200  $\mu\text{g/ml}$  for each sample, as well as using distal water (DW) as a negative control. The plates were wrapped with parafilm tape and incubated

at 37°C overnight. Negative controls using only *E.coli* and *S.aureus* were used. The inhibition zones of bacterial growth were then measured in millimeters [25, 26].

### 3. Results and Discussion

#### 3.1. Structural Properties

Figure 1(a,b) shows the X-Ray diffraction pattern of  $\text{Bi}_2\text{MoO}_6$  and  $\text{Bi}_2\text{WO}_6$  as generated by the hydrothermal method, respectively. As shown in Figure 1a, the (131), (200), (151), (202), (133) and (280) planes of the orthorhombic  $\text{Bi}_2\text{MoO}_6$  phase were responding to well-defined peaks at  $2\theta = 28^\circ, 32.4^\circ, 36^\circ, 46.6^\circ, 55.2^\circ, 56^\circ$ , respectively (JCPDS card no. 21-0102) [27]. Besides, there were no additional prominent peaks, confirming  $\text{Bi}_2\text{MoO}_6$  purity. The peaks at  $2\theta$  of  $27.8^\circ, 32.8^\circ, 47^\circ, 55.6^\circ, 58.4^\circ, 68.6^\circ$ , and  $75.6^\circ$  are assigned to (131), (200), (202), (133), (262) and (400) planes of orthorhombic  $\text{Bi}_2\text{WO}_6$  (JCPDS, No. 39-0256), respectively as shown in Figure 1b which are similar to patterns of  $\text{Bi}_2\text{MoO}_6$  sample revealing the  $\text{Bi}_2\text{WO}_6$  is also isomorphic [28]. Moreover, the diffraction peaks of  $\text{Bi}_2\text{WO}_6$  in the range of  $2\theta = 30\text{--}60^\circ$  are higher than those of  $\text{Bi}_2\text{MoO}_6$ . Besides, there were no other diffraction peaks that could have been caused by contaminants that indicate crystallinity [16].

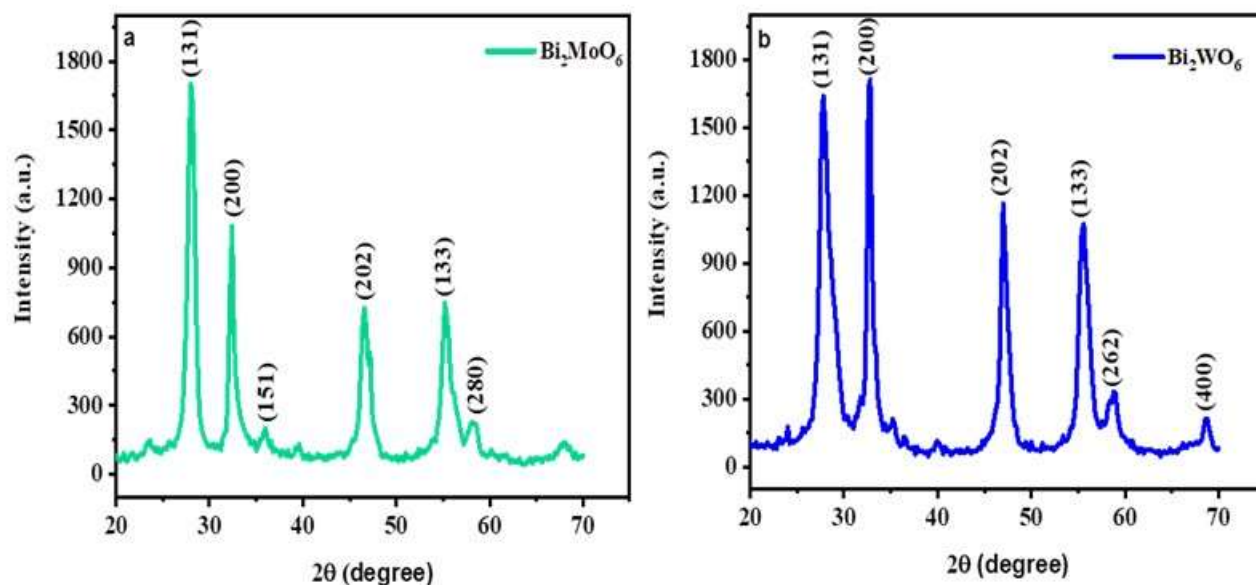


**Figure 1:** XRD patterns of the as-prepared a)  $\text{Bi}_2\text{MoO}_6$  and b)  $\text{Bi}_2\text{WO}_6$  products.

#### 3.2. Morphological Properties

FESEM was used to characterize the microstructure and morphology of  $\text{Bi}_2\text{MoO}_6$  and  $\text{Bi}_2\text{WO}_6$ . As shown in Figure 2a, the FESEM image of  $\text{Bi}_2\text{MoO}_6$  nanoparticles was made up of several uneven nanosheets or typical nanoplate like structures with smooth surfaces. Nanosheets were extremely thin with a thickness of 40-60 nm and an average width of approximately 300 nm. Furthermore, the nanosheets were tightly packed. Figure 2b, shows the FESEM image of the as-prepared  $\text{Bi}_2\text{WO}_6$ . This resulted in aggregated irregular tiny flake-like  $\text{Bi}_2\text{WO}_6$  that is made up of agglomerates of nanoplatelets with various orientations. The EDS spectrum of the  $\text{Bi}_2\text{MoO}_6$  and  $\text{Bi}_2\text{WO}_6$  samples were made to confirm the elemental composition and distribution homogeneity and are shown in Figures (c and d). Bi, Mo, and O components for  $\text{Bi}_2\text{MoO}_6$  and Bi, W, and O components for  $\text{Bi}_2\text{WO}_6$  are present throughout the entire samples. The homogenous distribution of each element in the matrix proves the samples' cleanliness.

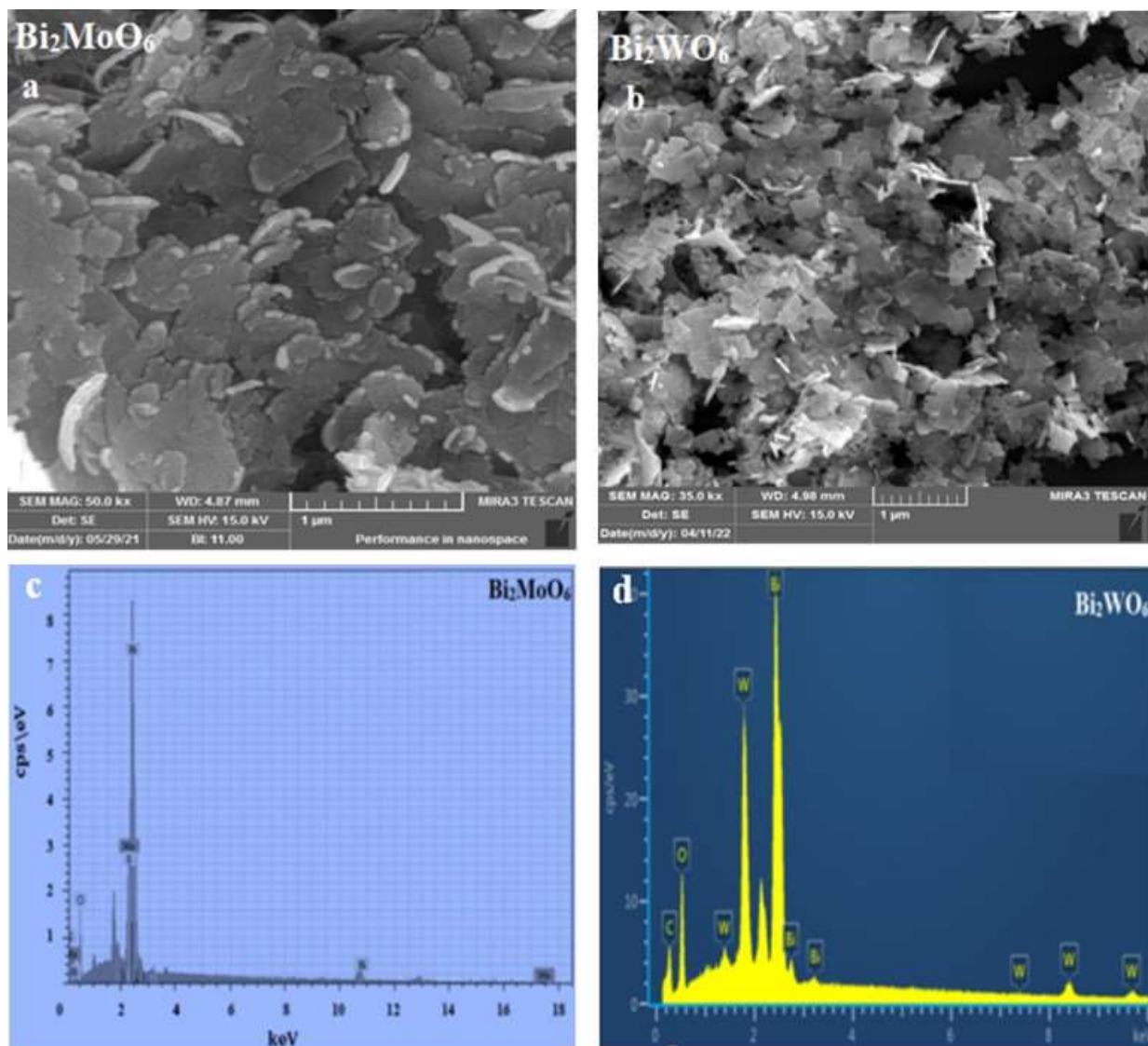


**Figure 2:** FESEM images (a) Bi<sub>2</sub>MoO<sub>6</sub>, (b) Bi<sub>2</sub>WO<sub>6</sub> and EDS images (c) Bi<sub>2</sub>MoO<sub>6</sub> and (d) Bi<sub>2</sub>WO<sub>6</sub> samples of prepared hydrothermal technique.

### 3.3. Optical Properties

The UV-Vis spectra analysis was carried out in the range of 240 – 700 nm to determine the optical properties of Bi<sub>2</sub>MoO<sub>6</sub> and Bi<sub>2</sub>WO<sub>6</sub>, respectively. As displayed in Figures 3 (a, b) and 4 (a, b), it was obvious that the photocatalyst had a strong absorption capacity in the visible light region. As can be seen from Figures 3 (a, b) and 4 (a, b), the absorption edges of Bi<sub>2</sub>MoO<sub>6</sub> and Bi<sub>2</sub>WO<sub>6</sub> were observed at about 300 nm and 400 nm, respectively. The absorption edge of Bi<sub>2</sub>MoO<sub>6</sub> is higher than that of Bi<sub>2</sub>WO<sub>6</sub>. In addition, as shown in Figures 3b and 4b, the band gaps of resulted samples Bi<sub>2</sub>MoO<sub>6</sub> and Bi<sub>2</sub>WO<sub>6</sub> were calculated using equation  $h\nu = A(h\nu - E_g)^n$  where absorption coefficient, photon energy, and general constant are all defined, as  $\alpha$ ,  $h\nu$  and  $A$ , respectively [29]. Using plotting  $\alpha h\nu$  against  $h\nu$  (Tauc-plot), then a tangent onto the linear range and extrapolation can be used to determine the band gaps.

### 3.4. Antibacterial Activity

To investigate the antibacterial activity of resulting Bi<sub>2</sub>MoO<sub>6</sub> and Bi<sub>2</sub>WO<sub>6</sub> samples against test bacteria strain *E.coli* and *S.aureus* bacteria, three different test concentrations (50, 100, and 200)  $\mu\text{g/ml}$  of each sample were incubated with bacterial strains at 37°C for overnight without irradiation, respectively. As shown in Figures 5a,

b and 7a, b, the results indicated that the tested bacterial strains, *S.aureus* revealed the highest zone of inhibition (24 to 29 mm) for  $\text{Bi}_2\text{MoO}_6$  and (17.5 to 21.5 mm) for  $\text{Bi}_2\text{WO}_6$  in the concentrations of 100  $\mu\text{g/ml}$ , 200  $\mu\text{g/ml}$ , respectively. While the less susceptible strain was found to be *E.coli* which revealed a smaller zone of inhibition (15.7 to 20.3mm) for  $\text{Bi}_2\text{MoO}_6$  and (12.6 to 18.7 mm) for  $\text{Bi}_2\text{WO}_6$  at concentrations of 100  $\mu\text{g/ml}$ , 200  $\mu\text{g/ml}$ , respectively.

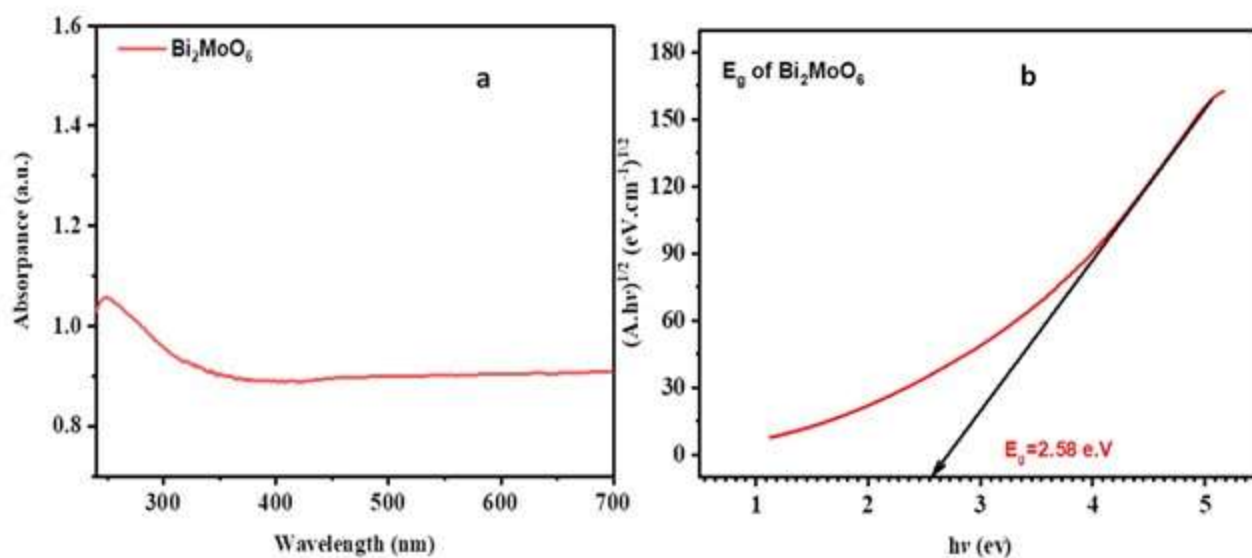


**Figure 3:** The UV-Vis analysis spectra of (a  $\text{Bi}_2\text{MoO}_6$ , (b energy gap  $E_g$  of  $\text{Bi}_2\text{MoO}_6$

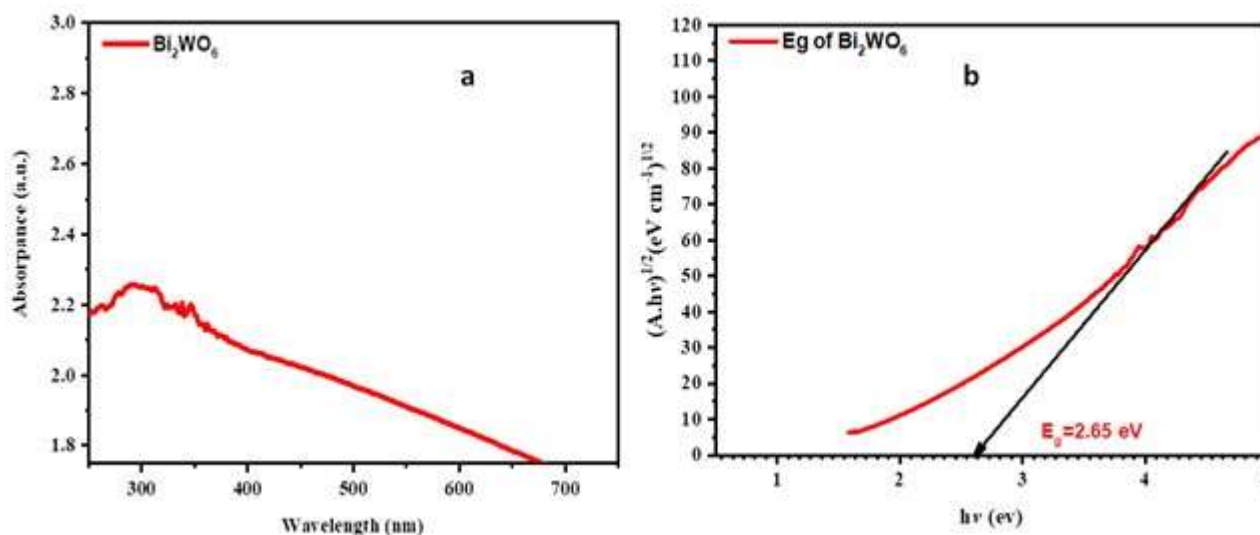


**Figure 4:** UV-Vis analysis spectra of (a  $\text{Bi}_2\text{WO}_6$ , and (b energy gap  $E_g$  of  $\text{Bi}_2\text{WO}_6$

No inhibition zone was detected for control (D.W) as shown in Figures 6 a,b and 8 a,b, respectively. Moreover, the results exhibited that the tested bacterial strain, *S.aureus* was the most susceptible bacterial strain revealing large zones of (24 mm to 29 mm) for  $\text{Bi}_2\text{MoO}_6$  and becoming less susceptible (17.5 to 21.5 mm) for  $\text{Bi}_2\text{WO}_6$  in the concentrations of 100  $\mu\text{g/ml}$ , 200  $\mu\text{g/ml}$ , respectively in comparison with the inhibition zone against tested bacterial *E.coli* as display in Figures 7 a,b and 8 a,b.

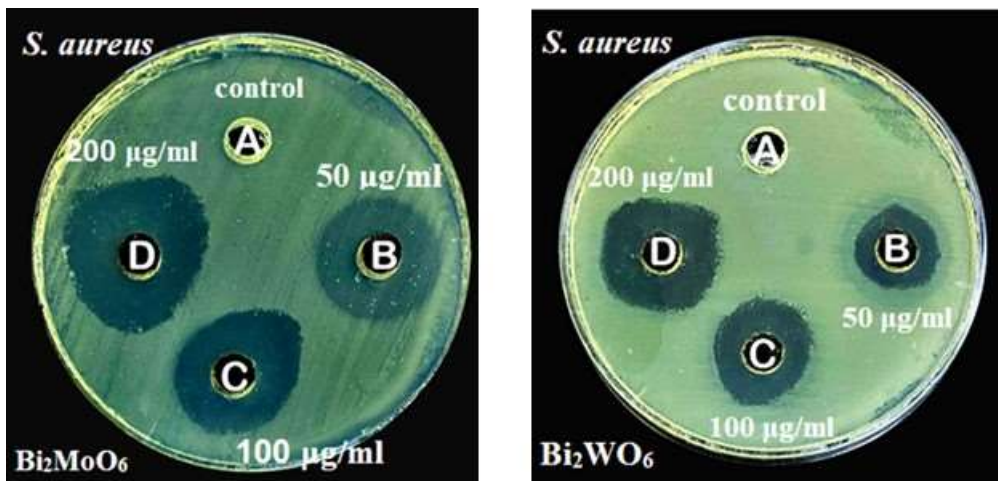


Figure 5: Images of inhibition Zone (mm) for a)  $\text{Bi}_2\text{MoO}_6$  and of b)  $\text{Bi}_2\text{WO}_6$  against *E.coli* bacterial strain.

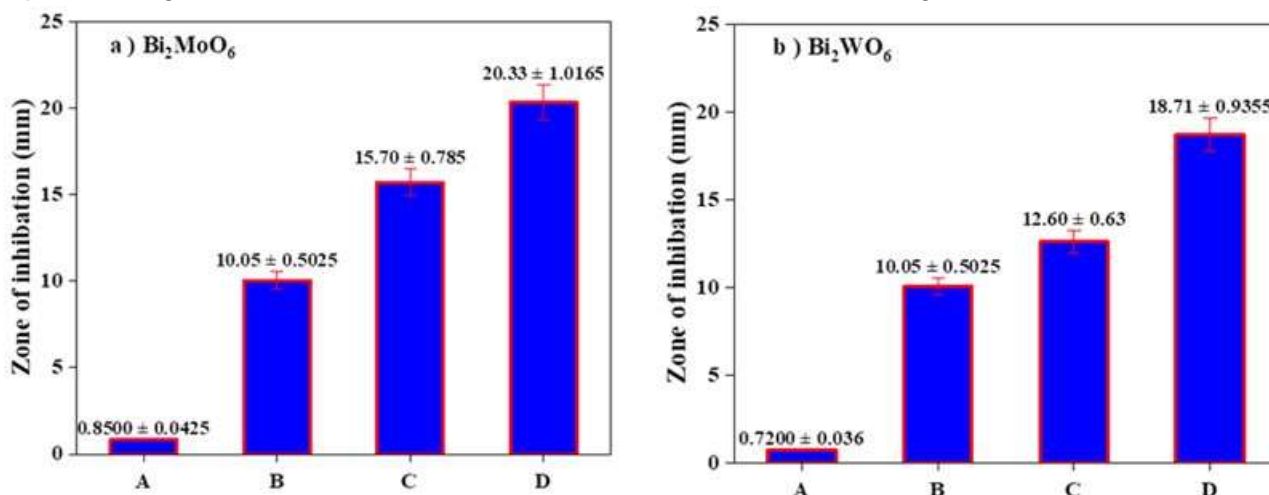


Figure 6: The Antibacterial activity of a)  $\text{Bi}_2\text{MoO}_6$  and b)  $\text{Bi}_2\text{WO}_6$  against *E.coli* using different content A)control, B) 50  $\mu\text{g/ml}$ , C) 100  $\mu\text{g/ml}$ , D) 200  $\mu\text{g/ml}$

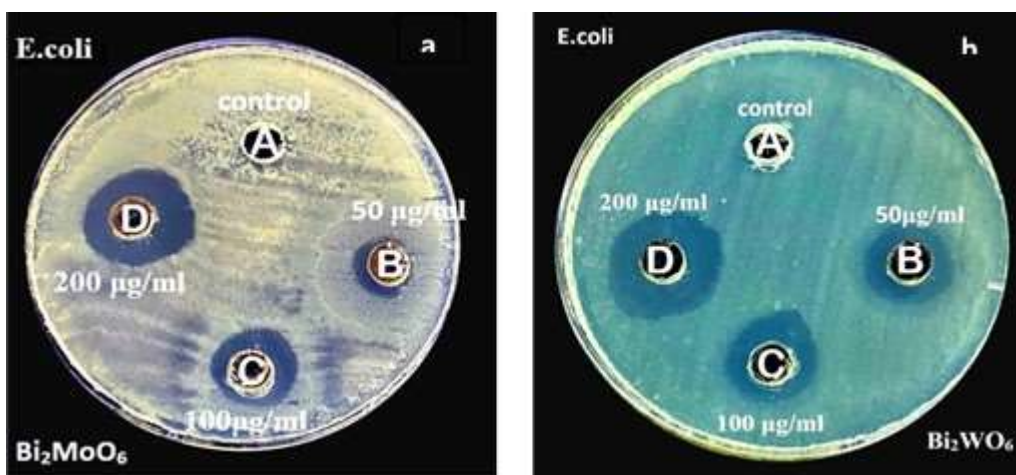
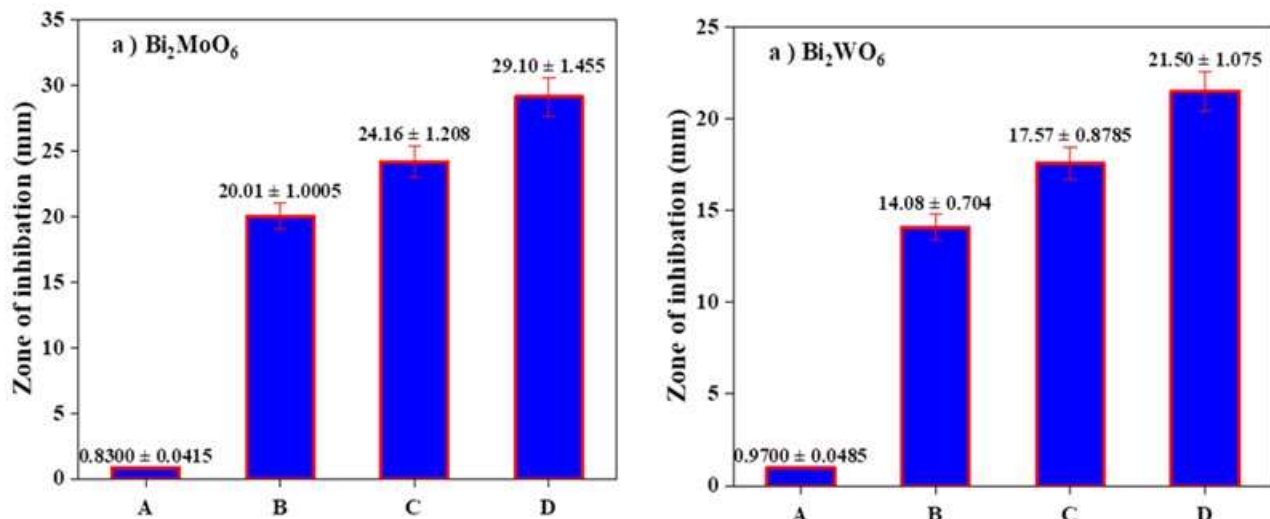


Figure7: Images of inhibition Zone (mm) for a)  $\text{Bi}_2\text{MoO}_6$  and of b)  $\text{Bi}_2\text{WO}_6$  against *S.aureus* bacterial strain

These results reveal that  $\text{Bi}_2\text{MoO}_6$  has strong antibacterial activity against *E.coli* and *S.aureus* bacteria related to possible mechanism dealing with penetration of cell membrane by  $\text{Bi}_2\text{MoO}_6$  nanosheets as compared with  $\text{Bi}_2\text{WO}_6$ , which results in oxidation of the bacterial membrane by the effective electrostatic force between Bi-based and bacterial surface and results in the leakage of the interior component as well as improved their resistance to biological contamination [29, 30]. In addition, the interesting point to underline is that the resulting samples  $\text{Bi}_2\text{MoO}_6$  and  $\text{Bi}_2\text{WO}_6$  exhibited a strong effect on gram-positive and gram-negative bacteria, which highlights the great clinical and technological application [24, 31].



**Figure 8:** The Antibacterial activity of a)  $\text{Bi}_2\text{MoO}_6$  and b)  $\text{Bi}_2\text{WO}_6$  against *S.aureus* sing different content A)control, B) 50 µg/ml, C) 100 µg/ml, D) 200 µg/ml

#### 4. Conclusions

$\text{Bi}_2\text{MoO}_6$  and  $\text{Bi}_2\text{WO}_6$  were synthesized by a hydrothermal method. The structure and morphology characterization of fabricated samples by using FESEM, EDS, and XRD reveals the formation of a nanosheet or nanoplate like structure with a smooth surface of each sample and the forming of orthorhombic  $\text{Bi}_2\text{MoO}_6$  and  $\text{Bi}_2\text{WO}_6$  phases without defects. Besides, a strong absorption capacity in the visible light region was exhibit of resulted in  $\text{Bi}_2\text{MoO}_6$  and  $\text{Bi}_2\text{WO}_6$ . Moreover, the antibacterial activity of  $\text{Bi}_2\text{MoO}_6$  and  $\text{Bi}_2\text{WO}_6$  was improved against *S.aureus* bacteria and became less susceptible against *E.coli* as well as the  $\text{Bi}_2\text{MoO}_6$  became highly susceptible against *E.coli* and *S.aureus* bacteria related to oxidation of the bacterial membrane by the effective electrostatic force between the Bi-based and bacterial surface.

#### Acknowledgments

We are grateful to Advanced Labs. in the center of nanotechnology, the University of Technology for their support of the work by making the biological tests in the Labs and providing us with the protocol for making these tests.

#### Conflict of Interest

No conflict

#### References

- [1] D. Lombardo, M. A. Kiselev, and M. T. Caccamo, "Smart Nanoparticles for Drug Delivery Application: Development of Versatile Nanocarrier Platforms in Biotechnology and Nanomedicine," *Journal of Nanomaterials*, vol. 2019, 2019, doi: 10.1155/2019/3702518.
- [2] S. M. H. Al-Jawad, Z. S. Shakir, and D. S. Ahmed, "Antibacterial activity of Nickel-doped ZnO/MWCNTs hybrid prepared by sol-gel technique," *European Physics Journal: Applied Physics.*, vol. 96, no. 2, 2021, doi: 10.1051/epjap/2021210115.

- [3] N. Xue, L. Wang, W. Li, S. Wang, X. Pan, and D. Zhang, "Increased inheritance of structure and function of bacterial communities and pathogen propagation in plastsphere along a river with increasing antibiotics pollution gradient," *Environmental Pollution*, vol. 265, p. 114641, 2020, doi: 10.1016/j.envpol.2020.114641.
- [4] R. He, D. Xu, B. Cheng, J. Yu, and W. Ho, "Review on nanoscale Bi-based photocatalysts," *Nanoscale Horizons*, vol. 3, no. 5, pp. 464–504, 2018, doi: 10.1039/c8nh00062j.
- [5] R. He, S. Cao, P. Zhou, and J. Yu, "Recent advances in visible light Bi-based photocatalysts," *Cuihua Xuebao/Recent advances in visible light Bi-based photocatalysts*, vol. 35, no. 7, pp. 989–1007, 2014, doi: 10.1016/s1872-2067(14)60075-9.
- [6] J. A. Byrne et al., "A review of heterogeneous photocatalysis for water and surface disinfection," *Molecules*, vol. 20, no. 4, pp. 5574–5615, 2015, doi: 10.3390/molecules20045574.
- [7] L. Rizzo, A. Della Sala, A. Fiorentino, and G. Li Puma, "Disinfection of urban wastewater by solar driven and UV lamp - TiO<sub>2</sub> photocatalysis: Effect on a multi drug resistant Escherichia coli strain," *Water Research*, vol. 53, no. 0, pp. 145–152, 2014, doi: 10.1016/j.watres.2014.01.020.
- [8] L. Zhang, W. Wang, Z. Chen, L. Zhou, H. Xu, and W. Zhu, "Fabrication of flower-like Bi<sub>2</sub>WO<sub>6</sub> superstructures as high performance visible-light driven photocatalysts," *Journal of Materials Chemistry*, vol. 17, no. 24, pp. 2526–2532, 2007, doi: 10.1039/b616460a.
- [9] D. Xia et al., "Enhanced photocatalytic inactivation of Escherichia coli by a novel Z-scheme g-C<sub>3</sub>N<sub>4</sub>/m-Bi<sub>2</sub>O<sub>4</sub> hybrid photocatalyst under visible light: The role of reactive oxygen species," *Applied Catalysis B: Environmental*, vol. 214, pp. 23–33, 2017, doi: 10.1016/j.apcatb.2017.05.035.
- [10] X. Wang, F. Gu, L. Li, G. Fang, and X. Wang, "A facile mixed-solvothermal route to  $\gamma$ -Bi<sub>2</sub>MoO<sub>6</sub> nanoflakes and their visible-light-responsive photocatalytic activity," *Materials Research Bulletin*, vol. 48, no. 10, pp. 3761–3765, 2013, doi: 10.1016/j.materresbull.2013.05.104.
- [11] L. Zhang, T. Xu, X. Zhao, and Y. Zhu, "Controllable synthesis of Bi<sub>2</sub>MoO<sub>6</sub> and effect of morphology and variation in local structure on photocatalytic activities," *Applied Catalysis B: Environmental*, vol. 98, no. 3–4, pp. 138–146, 2010, doi: 10.1016/j.apcatb.2010.05.022.
- [12] T. Saison et al., "New insights into Bi<sub>2</sub>WO<sub>6</sub> properties as a visible-light photocatalyst," *Journal Physics Chem. C*, vol. 117, no. 44, pp. 22656–22666, 2013, doi: 10.1021/jp4048192.
- [13] Giannakis, S. *et al.*, "Insights into the Photocatalytic Bacterial Inactivation by Flower-Like Bi<sub>2</sub>WO<sub>6</sub> under Solar or Visible Light," *Water*, vol. 12, no. 1, pp. 1–19, 2020. <https://doi.org/10.3390/w12041099>
- [14] W. Wang, G. Huang, J. C. Yu, and P. K. Wong, "Advances in photocatalytic disinfection of bacteria: Development of photocatalysts and mechanisms," *Journal of Environmental Sciences (China)*, vol. 34, pp. 232–247, 2015, doi: 10.1016/j.jes.2015.05.003.
- [15] J. Tang, Z. Zou, and J. Ye, "Photocatalytic decomposition of organic contaminants by Bi<sub>2</sub>WO<sub>6</sub> under visible light irradiation," *Catalysis Letters*, vol. 92, no. 1–2, pp. 53–56, 2004, doi: 10.1023/b:catl.0000011086.20412.aa.
- [16] S. Helali, M. I. Polo-Lopez, P. Fernandez-Ibanez, B. Ohtani, F. Amano, et al., "Effect of different types of suspended catalyst on Escherichia coli photocatalytic inactivation under natural sunlight .," no. August, 2015.
- [17] G. Tian et al., "Facile solvothermal synthesis of hierarchical flower-like Bi<sub>2</sub>MoO<sub>6</sub> hollow spheres as high performance visible-light driven photocatalysts," *Journal Materials Chemistry*, vol. 21, no. 3, pp. 887–892, 2011, doi: 10.1039/c0jm03040f.
- [18] R. Shen, C. Jiang, Q. Xiang, J. Xie, and X. Li, "Surface and interface engineering of hierarchical photocatalysts," *Applied Surface Science*, vol. 471, no. 31, pp. 43–87, 2019, doi: 10.1016/j.apsusc.2018.11.205.
- [19] H. N. Abid, A. Al-keisy, D. S. Ahmed, A. T. Salih, and A. Khammas, "pH dependent synthesis and characterization of bismuth molybdate nanostructure for photocatalysis degradation of organic pollutants," *Environmental Science and Pollution Research*, vol. 29, pp. 1–13, 2022, doi: 10.1007/s11356-021-18064-3.



- [20] H. H. Bahjat, R. A. Ismail, G. M. Sulaiman & M. S. Jabir “Magnetic Field – Assisted Laser Ablation of Titanium Dioxide Nanoparticles in Water for Anti- Bacterial Applications,” *Journal of Inorganic and Organometallic Polymers and Materials*, vol. 31, pp. 3649–3656 2021.
- [21] N. Ali, A. Taha, and D. Ahmed, “Characterization of Treated Multi-Walled Carbon Nanotubes and Antibacterial Properties,” *Journal of Applied Sciences and Nanotechnology*, vol. 1, no. 2, pp. 1–9, 2021, doi: 10.53293/jasn.2021.11636.
- [22] H. N Abid, D. S Ahmed and A. H Al-keisy, “Constructed p-2D / n-2D BiOCl / BiVO<sub>4</sub> Nanoheterostructure for Photocatalytic Antibacterial Activity,” *ECS Transactions*, 2022. DOI 10.1149/10701.2283ecst
- [23] D. S. Ahmed, N. Q. Ali, and A. A. Taha, “The Variation Effect of Mg-doped NPs Prepared by Sol-Gel Method on its Structural Properties and Biological Activities,” *Journal of Physics: Conference Series*, vol. 2114, no. 1, 2021, doi: 10.1088/1742-6596/2114/1/012004.
- [24] Q. Feng, J. Zhou, and Y. Zhang, “Coupling Bi<sub>2</sub>MoO<sub>6</sub> with persulfate for photocatalytic oxidation of tetracycline hydrochloride under visible light,” *Journal of Materials Science: Materials in Electronics*, vol. 30, no. 21, pp. 19108–19118, 2019, doi: 10.1007/s10854-019-02266-0.
- [25] C. Zhu, Y. Liu, H. Cao, J. Sun, Q. Xu, and L. Wang, “Insight into the influence of morphology of Bi WO<sub>6</sub> for photocatalytic degradation of VOCs under visible light,” *Colloids and Surfaces A: Physicochemical and Engineering Aspects*, vol. 568, no. February, pp. 327–333, 2019, doi: 10.1016/j.colsurfa.2019.02.029.
- [26] J. Jia et al., “Highly efficient and stable Au/Bi<sub>2</sub>MoO<sub>6</sub>/Bi<sub>2</sub>WO<sub>6</sub> heterostructure with enhanced photocatalytic activity for NO gas removal under visible light irradiation,” *Journal of Physics D: Applied Physics*, vol. 50, no. 14, 2017, doi: 10.1088/1361-6463/aa60e3.
- [27] J. Liang, F. Liu, J. Deng, M. Li, and M. Tong, “Efficient bacterial inactivation with Z-scheme AgI/Bi<sub>2</sub>MoO<sub>6</sub> under visible light irradiation,” *Water Research*, vol. 123, pp. 632–641, 2017, doi: 10.1016/j.watres.2017.06.060.
- [28] B. Li et al., “Superimposed surface plasma resonance effect enhanced the near-infrared photocatalytic activity of Au@Bi<sub>2</sub>WO<sub>6</sub> coating for rapid bacterial killing,” *Journal of Hazardous Materials*, vol. 380, no. July, 2019, doi: 10.1016/j.jhazmat.2019.120818.
- [29] P. Kanniah et al., “ Green Synthesis of Multifaceted Silver Nanoparticles Using the Flower Extract of *Aerva lanata* and Evaluation of Its Biological and Environmental Applications ,” *ChemistrySelect*, vol. 5, no. 7, pp. 2322–2331, 2020, doi: 10.1002/slct.201903228.
- [30] S. Ahmed, M. Ahmad, B. L. Swami, and S. Ikram, “A review on plants extract mediated synthesis of silver nanoparticles for antimicrobial applications: A green expertise,” *Journal of Advanced Research*, vol. 7, no. 1, pp. 17–28, 2016, doi: 10.1016/j.jare.2015.02.007.
- [31] Z. Khedaer, D. Ahmed, and S. Al-Jawad, “Investigation of Morphological, Optical, and Antibacterial Properties of Hybrid ZnO-MWCNT Prepared by Sol-gel,” *Journal of Applied Sciences and Nanotechnology*, vol. 1, no. 2, pp. 66–77, 2021, doi: 10.53293/jasn.2021.11634.